Belalia *Mechanics of Advanced Materials and Modern Processes* (2017) 3:4
DOI 10.1186/s40759-017-0018-0

Mechanics of Advanced Materials and Modern Processes

RESEARCH Open Access

Linear and non-linear vibration analysis of moderately thick isosceles triangular FGPs using a triangular finite p-element

SA. Belalia

Abstract

Background: The geometrically non-linear formulation based on Von-Karman's hypothesis is used to study the free vibration isosceles triangular plates by using four types of mixtures of functionally graded materials (FGMs - AL/AL_2O_3, SUS304/Si_3N_4, Ti- AL-4V/Aluminum oxide, AL/ZrO_2). Material properties are assumed to be temperature dependent and graded in the thickness direction according to power law distribution.

Methods: A hierarchical finite element based on triangular p-element is employed to define the model, taking into account the hypotheses of first-order shear deformation theory. The equations of non-linear free motion are derived from Lagrange's equation in combination with the harmonic balance method and solved iteratively using the linearized updated mode method.

Results: Results for the linear and nonlinear frequencies parameters of clamped isosceles triangular plates are obtained. The accuracy of the present results are established through convergence studies and comparison with results of literature for metallic plates. The results of the linear vibration of clamped FGMs isosceles triangular plates are also presented in this study.

Conclusion: The effects of apex angle, thickness ratio, volume fraction exponent and mixtures of FGMs on the backbone curves and mode shape of clamped isosceles triangular plates are studied. The results obtained in this work reveal that the physical and geometrical parameters have a important effect on the non-linear vibration of FGMs triangular plates.

Keywords: The mixtures effect of Ceramic-Metal, Linear and Non-linear vibration, Moderately thick FGM plates, *p*-version of finite element method

Background

In recent years, the geometrically non-linear vibration of functionally graded Materials (FGMs) for different structures has acquired great interest in many researches. In 1984, The concept of the FGMs was introduced in Japan by scientific researchers (Koizumi 1993; Koizumi 1997). FGMs are composite materials which are microscopically inhomogeneous. The mechanical properties of FGMs are expressed with mathematical functions, and assumed to vary continuously from one surface to the other.

Since the variation of mechanical properties of FGM is nonlinear, therefore, studies based on the nonlinear deformation theory is required for these type of materials. Many works have studied the static and dynamic nonlinear behavior of functionally graded plates with various shapes. The group of researchers headed by (Reddy and Chin 1998; Reddy et al. 1999; Reddy 2000) have done a lot of numerical and theoretical work on FG plates under several effects (thermoelastic response, axisymmetric bending and stretching, finite element models, FSDT-plate and TSDT-plate). Woo & Meguid (2001) analyzed the nonlinear behavior of functionally graded shallow shells and thin plates under temperature effects and mechanical loads. The analysis of nonlinear bending of FG simply supported rectangular plates submissive to thermal and mechanical loading was studied by (Shen 2002). (Huang & Shen 2004) applied the perturbation technique to nonlinear vibration and dynamic response of FG plates in a thermal environment. Chen (2005) investigated the large amplitude vibration of FG plate with arbitrary initial stresses based on FSDT. An

Correspondence: belaliasidou@yahoo.fr
Faculty of Technology, Department of Mechanical Engineering, University of Tlemcen, B.P. 230, Tlemcen 13000, Algeria

analytical solution was proposed by Woo et al. 2006 to analyzed the nonlinear vibration of functionally graded plates using classic plate theory. Allahverdizadeh et al. (2008a, 2008b) have studied the non-linear forced and free vibration analysis of circular functionally graded plate in thermal environment. The *p*-version of the FEM has been applied to investigate the non-linear free vibration of elliptic sector plates and functionally graded sector plates by (Belalia & Houmat 2010; 2012). Hao et al. 2011 analyzed the non-linear vibration of a cantilever functionally graded plate based on TSDT of plate and asymptotic analysis and perturbation method. Duc & Cong 2013 analyzed the non-linear dynamic response of imperfect symmetric thin sandwich FGM plate on elastic foundation. Yin et al. 2015 proposed a novel approach based on isogeometric analysis (IGA) for the geometrically nonlinear analysis of functionally graded plates (FGPs). the same approach (IGA) and a simple first-order shear deformation plate theory (S-FSDT) are used by Yu et al. 2015 to investigated geometrically nonlinear analysis of homogeneous and non-homogeneous functionally graded plates. Alinaghizadeh & Shariati 2016, investigated the non-linear bending analysis of variable thickness two-directional FG circular and annular sector plates resting on the non-linear elastic foundation using the generalized differential quadrature (GDQ) and the Newton–Raphson iterative methods.

The *p*-version FEM has many advantages over the classic finite element method (*h*-version), which includes the ability to increase the accuracy of the solution without re-defining the mesh (Han & Petyt 1997; Ribeiro 2003). This advantage is suitable in non-linear study because the problem is solved iteratively and the nonlinear stiffness matrices are reconstructed throughout each iteration. Using the *p*-version with higher order polynomials, the structure is modeled by one element while satisfying the exactitude requirement. In *p*-version, the point where the maximum amplitude is easy to find it as there is a single element, contrary to the *h*-version this point must be sought in every element of the mesh which is very difficult. The advantages of the *p*-version mentioned previously, make it more powerful to the nonlinear vibration analysis of plates. So far, no work has been published to the study of linear and nonlinear vibration of FGMs isosceles triangular plate by using the *p*-version of FEM.

In the present work, the non-linear vibration analysis of moderately thick FGMs isosceles triangular plates was investigated by a triangular finite *p*-element. The shape functions of triangular finite *p*-element are obtained by the shifted orthogonal polynomials of Legendre. The effects of rotatory inertia and transverse shear deformations are taken into account (Mindlin 1951). The Von-Karman hypothesis are used in combination with the harmonic balance method (HBM) to obtained the motion equations. The resultant equations of motion are solved iteratively using the linearized updated mode method. The exactitude of the p-element is investigated with a clamped metallic triangular plate. Comparisons are made between current results and those from published results. The effects of thickness ratio, apex angle, exponent of volume fraction and mixtures of FGMs on the backbone curves and mode shape of clamped isosceles triangular plates are also studied.

Methods

Consider a moderately thick isosceles triangular plate with the following geometrical parameters thickness h, base b, height a and apex angle β (Fig. 1). The triangular p-element is mapped to global coordinates from the local coordinates ξ and η. The differential relationship between the two coordinates systems is given as a function of the Jacobian matrix ($\boldsymbol{J}$) by

$$\begin{Bmatrix} \frac{\partial}{\partial \xi} \\ \frac{\partial}{\partial \eta} \end{Bmatrix} = \boldsymbol{J} \begin{Bmatrix} \frac{\partial}{\partial x} \\ \frac{\partial}{\partial y} \end{Bmatrix} \tag{1}$$

where $\boldsymbol{J}$ is given by

$$\boldsymbol{J} = \begin{bmatrix} \frac{\partial x}{\partial \xi} & \frac{\partial y}{\partial \xi} \\ \frac{\partial x}{\partial \eta} & \frac{\partial y}{\partial \eta} \end{bmatrix} = \begin{bmatrix} b & 0 \\ b/2 & b/2tg\left(\frac{\beta}{2}\right) \end{bmatrix} \tag{2}$$

In first-order shear deformation plate theory, the displacements (u, v and w) at a point with coordinate (x, y, z) from the median surface are given as functions of

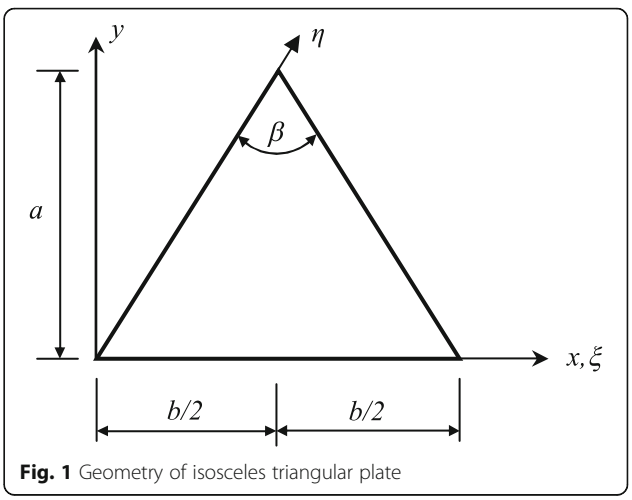

Fig. 1 Geometry of isosceles triangular plate

midplane displacements (u_0, v_0, w) and independent rotations (θ_x and θ_y) about the x and y axes as

$$\begin{aligned} u(x,y,z,t) &= u_0(x,y,t) + z\theta_y(x,y,t) \\ v(x,y,z,t) &= v_0(x,y,t) - z\theta_x(x,y,t) \\ w(x,y,z,t) &= w(x,y,t) \end{aligned} \tag{3}$$

The in-plane displacements (u, v) and out-of-plane displacements (w, θ_x and θ_y) will be expressed using the p-version FEM as

$$\begin{Bmatrix} u \\ v \end{Bmatrix} = \begin{bmatrix} N(\xi,\eta) & 0 \\ 0 & N(\xi,\eta) \end{bmatrix} \begin{Bmatrix} q_u \\ q_v \end{Bmatrix} \tag{4}$$

$$\begin{Bmatrix} w \\ \theta_y \\ \theta_x \end{Bmatrix} = \begin{bmatrix} N(\xi,\eta) & 0 & 0 \\ 0 & N(\xi,\eta) & 0 \\ 0 & 0 & N(\xi,\eta) \end{bmatrix} \begin{Bmatrix} q_w \\ q_{\theta_y} \\ q_{\theta_x} \end{Bmatrix} \tag{5}$$

where q_u, q_v are the vectors of generalized in-plane displacements, q_w, q_{θ_y} and q_{θ_x} are the vectors of generalized transverse displacement and rotations, respectively, $N(\xi,\eta)$ are the hierarchical shape functions of triangular p-element (Belalia & Houmat 2010).

Using FSDT of plate in combination with Von-Karman hypothesis, the nonlinear strain–displacement relationships are expressed as

$$\{\varepsilon\} = \{\varepsilon^L\} + \{\varepsilon^{NL}\} \tag{6}$$

where the linear and the non-linear strains can be expressed as,

$$\{\varepsilon^L\} = \begin{Bmatrix} \varepsilon_P^L \\ 0 \end{Bmatrix} + \begin{Bmatrix} z\varepsilon_b \\ \varepsilon_s \end{Bmatrix} \quad \text{and} \quad \{\varepsilon^{NL}\} = \begin{Bmatrix} \varepsilon_P^{NL} \\ 0 \end{Bmatrix} \tag{7}$$

the components of linear and the non-linear strains given in Eq. (7) are defined as

Table 1 Mechanical properties of FGMs components Yang et al. (2003) and Zhao et al. (2009)

Material	Properties		
	E (10^9 N/m^2)	ν	ρ (kg/m^3)
Aluminium (Al)	70.00	0.30	2707
Alumina (Al_2O_3)	380.00	0.30	3800
Stainless steel SUS304	207.78	0.3177	8166
Silicon nitride Si_3N_4	322.27	0.24	2370
Ti-6AL-4 V	105.7	0.2981	4429
Aluminum oxide	320.24	0.26	3750
Zirconia (ZrO_2)	151.00	0.30	3000

Table 2 Convergence of the first three linear frequency parameters for clamped metallic isosceles triangular plate ($\beta = 90°$)

h/b	Mode	p					
		6	7	8	9	10	11
0.05	Ω_1	166.3	164.6	164.4	164.3	164.3	164.3
	Ω_2	277.2	265.7	261.9	261.1	260.9	260.9
	Ω_3	330.4	321.2	316.3	314.3	313.8	313.7
0.1	Ω_1	128.2	127.9	127.9	127.9	127.9	127.9
	Ω_2	195.1	191.2	190.5	190.2	190.2	190.2
	Ω_3	227.9	225.0	223.6	223.3	223.2	223.2
0.15	Ω_1	100.3	100.2	100.2	100.2	100.2	100.2
	Ω_2	146.1	144.3	144.1	144.0	144.0	144.0
	Ω_3	168.7	167.4	166.8	166.7	166.7	166.7

$$\{\varepsilon_P^L\} = \begin{Bmatrix} \dfrac{\partial u}{\partial x} \\ \dfrac{\partial v}{\partial y} \\ \dfrac{\partial u}{\partial y} + \dfrac{\partial v}{\partial x} \end{Bmatrix}, \quad \{\varepsilon_b\} = \begin{Bmatrix} \dfrac{\partial \theta_y}{\partial x} \\ -\dfrac{\partial \theta_x}{\partial y} \\ \dfrac{\partial \theta_y}{\partial y} - \dfrac{\partial \theta_x}{\partial x} \end{Bmatrix} \tag{8}$$

$$\{\varepsilon_s\} = \begin{Bmatrix} \dfrac{\partial w}{\partial x} + \theta_y \\ \dfrac{\partial w}{\partial y} - \theta_x \end{Bmatrix} \quad \{\varepsilon_P^{NL}\} = \begin{Bmatrix} \dfrac{1}{2}\left(\dfrac{\partial w}{\partial x}\right)^2 \\ \dfrac{1}{2}\left(\dfrac{\partial w}{\partial y}\right)^2 \\ \dfrac{\partial w}{\partial x}\dfrac{\partial w}{\partial y} \end{Bmatrix} \tag{9}$$

The differential relationship used in Eqs. 8–9 is obtained by inversing Eq. 1 as

$$\begin{Bmatrix} \dfrac{\partial}{\partial x} \\ \dfrac{\partial}{\partial y} \end{Bmatrix} = \boldsymbol{J}^{-1} \begin{Bmatrix} \dfrac{\partial}{\partial \xi} \\ \dfrac{\partial}{\partial \eta} \end{Bmatrix} \tag{10}$$

Table 3 Comparison of the first three linear frequency parameters for clamped metallic isosceles triangular plate

h/b	Mode	β					
		30°		60°		90°	
		Present	Liew et al. (1998)	Present	Liew et al. (1998)	Present	Liew et al. (1998)
0.05	Ω_1	51.55	*51.55*	91.86	*91.86*	164.3	*164.4*
	Ω_2	80.60	*80.61*	167.5	*167.5*	260.9	*260.9*
	Ω_3	109.5	*109.5*	167.5	*167.5*	313.7	*313.7*
0.1	Ω_1	46.35	*46.35*	77.76	*77.79*	127.9	*127.9*
	Ω_2	69.82	*69.81*	132.3	*132.3*	190.2	*190.3*
	Ω_3	92.16	*92.17*	132.3	*132.3*	223.1	*223.2*
0.15	Ω_1	40.55	*40.55*	64.58	*64.59*	100.2	*100.2*
	Ω_2	59.07	*59.07*	104.7	*104.7*	143.0	*144.0*
	Ω_3	76.12	*76.15*	104.7	*104.7*	166.7	*166.7*

The strain energy E_S and kinetic energy E_K of the functionally graded moderately thick plate can expressed as

$$E_S = \frac{1}{2}\iint\Big[\{\varepsilon_p\}^{\mathrm{T}}[\mathrm{A_{ij}}]\{\varepsilon_p\} + \{\varepsilon_p\}^{\mathrm{T}}[\mathrm{B_{ij}}]\{\varepsilon_b\} + \{\varepsilon_b\}^{T}[B_{ij}]\{\varepsilon_p\} + \{\varepsilon_b\}^{T}[D_{ij}]\{\varepsilon_b\} + \{\varepsilon_s\}^{T}[S_{ij}]\{\varepsilon_s\}\Big]dxdy \tag{11}$$

$$E_K = \frac{1}{2}\iint\left[I_1\left(\left(\frac{\partial u}{\partial t}\right)^2 + \left(\frac{\partial v}{\partial t}\right)^2 + \left(\frac{\partial w}{\partial t}\right)^2\right) + I_3\left(\left(\frac{\partial \theta_x}{\partial t}\right)^2 + \left(\frac{\partial \theta_y}{\partial t}\right)^2\right)\right]dxdy \tag{12}$$

where $[A_{ij}]$, $[B_{ij}]$ and $[D_{ij}]$, are extensional, bending-extensional and bending stiffness constants of the FG plate and are given by

$$\left[A_{ij}, B_{ij}, D_{ij}\right] = \int_{-\frac{h}{2}}^{+\frac{h}{2}} Q_{ij}\left(1, z, z^2\right)dz \quad (i,j = 1,2,6) \tag{13}$$

$$\left[S_{ij}\right] = k\int_{-\frac{h}{2}}^{+\frac{h}{2}} Q_{ij}dz \quad (i,j = 4,5) \tag{14}$$

where k is a shear correction factor and is equal to $\pi^2/12$

Table 4 The first three linear frequency parameters of clamped FG AL/AL_2O_3 isosceles triangular plate

β	h/b	Mode	n							
			ceramic	0.1	0.5	1	2	5	10	metal
30°	0.05	Ω_{L1}	5.0681	4.8827	4.3399	3.9585	3.6367	3.4112	3.2521	2.5773
		Ω_{L2}	7.9247	7.6385	6.8050	6.2214	5.7244	5.3517	5.0840	4.0300
		Ω_{L3}	10.768	10.382	9.2453	8.4385	7.7440	7.2297	6.8741	5.4761
	0.1	Ω_{L1}	9.1144	8.7992	7.8656	7.1908	6.5871	6.0926	5.7606	4.6349
		Ω_{L2}	13.729	13.267	11.904	10.916	10.009	9.1978	8.6491	6.9818
		Ω_{L3}	18.122	17.522	15.727	14.401	13.158	12.049	11.330	9.2160
	0.15	Ω_{L1}	11.960	11.571	10.404	9.5364	8.7114	7.9458	7.4521	6.0824
		Ω_{L2}	17.422	16.873	15.237	14.013	12.812	11.599	10.814	8.8598
		Ω_{L3}	22.452	21.759	19.656	18.046	16.436	14.823	13.822	11.418
60°	0.05	Ω_{L1}	9.0322	8.7089	7.7700	7.1137	6.5499	6.1081	5.7894	4.5931
		Ω_{L2}	16.471	15.893	14.197	12.987	11.922	11.066	10.472	8.3760
		Ω_{L3}	16.471	15.895	14.220	13.039	11.998	11.121	10.501	8.3760
	0.1	Ω_{L1}	15.290	14.785	13.290	12.200	11.179	10.225	9.5914	7.7757
		Ω_{L2}	26.023	25.197	22.727	20.880	19.081	17.304	16.159	13.233
		Ω_{L3}	26.023	25.197	22.734	20.895	19.098	17.307	16.159	13.233
	0.15	Ω_{L1}	19.048	18.460	16.696	15.361	14.020	12.629	11.751	9.6867
		Ω_{L2}	30.889	29.973	27.193	25.036	22.785	20.357	18.876	15.708
		Ω_{L3}	30.889	29.974	27.208	25.070	22.840	20.408	18.904	15.708
90°	0.05	Ω_{L1}	16.158	15.597	13.957	12.793	11.760	10.885	10.273	8.2171
		Ω_{L2}	25.654	24.788	22.260	20.454	18.802	17.278	16.227	13.046
		Ω_{L3}	30.842	29.806	26.705	24.420	22.326	20.519	19.338	15.684
	0.1	Ω_{L1}	25.141	24.354	22.002	20.236	18.487	16.701	15.561	12.785
		Ω_{L2}	37.407	36.275	32.868	30.265	27.597	24.749	22.981	19.022
		Ω_{L3}	43.879	42.565	38.556	35.441	32.237	28.877	26.830	22.314
	0.15	Ω_{L1}	29.543	28.682	26.067	24.026	21.861	19.453	17.991	15.023
		Ω_{L2}	42.470	41.260	37.557	34.620	31.440	27.861	25.732	21.597
		Ω_{L3}	49.166	47.778	43.507	40.090	36.371	32.198	29.726	25.002

$$Q_{11} = Q_{22} = \frac{E(z)}{1-\nu^2(z)} \quad Q_{12} = \nu(z)Q_{11} \quad Q_{44} = Q_{55} = Q_{66} = \frac{E(z)}{2(1+\nu(z))} \tag{15}$$

$$(I_1, I_3) = \int_{-h/2}^{+h/2} \rho(z)\left(1, z^2\right)dz \tag{16}$$

The material properties *E(z),ν(z),* and *ρ(z)* of the functionally graded triangular plate assumed to be graded only in the thickness direction according to a simple power law distribution in terms of the volume fraction of the constituents which is expressed a

$$E(z) = \quad (E_c - E_m)\left(\frac{1}{2} + \frac{z}{h}\right)^n + E_m \tag{17}$$

$$\nu(z) = \quad (\nu_c - \nu_m)\left(\frac{1}{2} + \frac{z}{h}\right)^n + \nu_m \tag{18}$$

$$\rho(z) = \quad (\rho_c - \rho_m)\left(\frac{1}{2} + \frac{z}{h}\right)^n + \rho_m \tag{19}$$

where *c* and *m* index designate the ceramic and the metal, respectively, *n* is the exponent of the volume fraction ($n \geq 0$), *z* is the thickness coordinate variable, *E* elastic modulus, *ρ* mass density, *h* is the thickness of the plate and *ν* is the Poisson's ratio. The bottom layer of the functionally graded triangular plate is fully metallic material and the top layer is fully ceramic material. The constants of material for four types of FGMs considered in this study (AL/AL_2O_3,-$SUS304/Si_3N_4$, Ti-6AL-4 V/Aluminum oxide, AL/ZrO_2) are shown in Table 1.

Inserting Eqs. (11–12) in Lagrange's equations the equations of free motion are obtained as:

Table 5 The first three linear frequency parameters of clamped FG $SUS304/Si_3N_4$ isosceles triangular plate

β	*h/b*	Mode	*n*							
			ceramic	0.1	0.5	1	2	5	10	metal
30°	0.05	Ω_{L1}	5.8366	5.1789	4.0506	3.5610	3.2026	2.9134	2.7785	2.5747
		Ω_{L2}	9.1371	8.1064	6.3395	5.5721	5.0090	4.5535	4.3414	4.0244
		Ω_{L3}	12.427	11.024	8.6199	7.5746	6.8066	6.1846	5.8959	5.4669
	0.1	Ω_{L1}	10.564	9.3705	7.3225	6.4269	5.7626	5.2220	4.9759	4.6207
		Ω_{L2}	15.956	14.149	11.053	9.6966	8.6850	7.8582	7.4845	6.9544
		Ω_{L3}	21.102	18.708	14.609	12.811	11.465	10.363	9.8682	9.1743
	0.15	Ω_{L1}	13.954	12.374	9.6609	8.4647	7.5657	6.8293	6.5019	6.0512
		Ω_{L2}	20.390	18.075	14.106	12.353	11.028	9.9374	9.4558	8.8055
		Ω_{L3}	26.332	23.336	18.2050	15.934	14.212	12.793	12.170	11.341
60°	0.05	Ω_{L1}	10.423	9.2477	7.2314	6.3544	5.7096	5.1871	4.9454	4.5855
		Ω_{L2}	19.056	16.902	13.210	11.601	10.413	9.4482	9.0049	8.3552
		Ω_{L3}	19.056	16.902	13.211	11.603	10.415	9.4492	9.0053	8.3552
	0.1	Ω_{L1}	17.805	15.790	12.331	10.810	9.6719	8.7402	8.3229	7.7404
		Ω_{L2}	30.433	26.975	21.052	18.440	16.469	14.849	14.131	13.156
		Ω_{L3}	30.433	26.975	21.053	18.441	16.470	14.850	14.132	13.156
	0.15	Ω_{L1}	22.345	19.812	15.456	13.522	12.053	10.845	10.318	9.6205
		Ω_{L2}	36.377	32.233	25.130	21.971	19.558	17.564	16.700	15.581
		Ω_{L3}	36.377	32.234	25.132	21.975	19.562	17.566	16.701	15.581
90°	0.05	Ω_{L1}	18.711	16.598	12.972	11.388	10.216	9.2627	8.8272	8.1943
		Ω_{L2}	29.792	26.422	20.641	18.112	16.227	14.689	13.992	12.998
		Ω_{L3}	35.858	31.808	24.843	21.792	19.508	17.650	16.8101	15.621
	0.1	Ω_{L1}	29.448	26.111	20.374	17.831	15.906	14.324	13.631	12.704
		Ω_{L2}	43.964	38.964	30.385	26.577	23.679	21.289	20.248	18.882
		Ω_{L3}	51.630	45.755	35.676	31.196	27.781	24.961	23.736	22.141
	0.15	Ω_{L1}	34.858	30.906	24.089	21.036	18.693	16.762	15.937	14.894
		Ω_{L2}	50.223	44.496	34.666	30.273	26.895	24.098	22.903	21.397
		Ω_{L3}	58.180	51.535	40.150	35.064	31.148	27.898	26.509	24.766

$$[\overline{M}]\begin{Bmatrix}\ddot{q}_u\\ \ddot{q}_v\end{Bmatrix}+[\overline{K}]\begin{Bmatrix}q_u\\ q_v\end{Bmatrix}+[\breve{K}+\hat{K}]\begin{Bmatrix}q_w\\ q_{\theta_y}\\ q_{\theta_x}\end{Bmatrix}=0 \quad (20)$$

$$[M]\begin{Bmatrix}\ddot{q}_w\\ \ddot{q}_{\theta_y}\\ \ddot{q}_{\theta_x}\end{Bmatrix}+[\tilde{K}+K]\begin{Bmatrix}q_w\\ q_{\theta_y}\\ q_{\theta_x}\end{Bmatrix}+\left[2\hat{K}+K\right]\begin{Bmatrix}\breve{q}_u\\ q_v\end{Bmatrix}=0 \quad (21)$$

The vector of generalized displacement in free motion will be given as

$$\begin{Bmatrix}q_w\\ q_{\theta_y}\\ q_{\theta_x}\end{Bmatrix}=\begin{Bmatrix}Q_w\\ Q_{\theta_y}\\ Q_{\theta_x}\end{Bmatrix}cos(\omega t)=Qcos(\omega t) \quad (22)$$

By neglecting the in-plane inertia, and taking into account the effects of the transverse shear deformation and inertia of rotation. Inserting Eqs. (20) and (22) into Eq. (21) and applying the HB-method, the final equation of free motion are of the form

$$[-\omega^2 M+K-\breve{K}^T\overline{K}^{-1}\breve{K}]\begin{Bmatrix}Q_w\\ Q_{\theta_y}\\ Q_{\theta_x}\end{Bmatrix} \quad (23)$$

$$+\frac{3}{4}\begin{bmatrix}\tilde{K}-2\hat{K}^T\overline{K}^{-1}\hat{K} & 0 & 0\\ 0 & 0 & 0\\ 0 & 0 & 0\end{bmatrix}\begin{Bmatrix}Q_w\\ Q_{\theta_y}\\ Q_{\theta_x}\end{Bmatrix}=0$$

Where M is the out-of-plane inertia matrices, $\overline{K}$, K and $\breve{K}$ are the extension, bending and coupled extension-rotation linear stiffness matrices, $\tilde{K}$ and $\hat{K}$ represent the nonlinear stiffness matrices. These matrices are given in Appendix A.

The system of equations given in Eq. (23) are solved iteratively using the linearized updated mode method. This

Table 6 The first three linear frequency parameters of clamped FG Ti-6AL-4 V/Aluminum oxide isosceles triangular plate

β	h/b	Mode	n							
			ceramic	0.1	0.5	1	2	5	10	metal
30°	0.05	Ω_{L1}	4.8290	4.6023	4.0178	3.6640	3.3821	3.1477	2.9915	2.5775
		Ω_{L2}	7.5568	7.2037	6.2958	5.7453	5.3021	4.9231	4.6728	4.0305
		Ω_{L3}	10.275	9.7962	8.5595	7.8050	7.1942	6.6742	6.3363	5.4770
	0.1	Ω_{L1}	8.7224	8.3224	7.2851	6.6421	6.1042	5.6259	5.3293	4.6364
		Ω_{L2}	13.162	12.565	11.018	10.053	9.2288	8.4668	8.0039	6.9847
		Ω_{L3}	17.397	16.613	14.569	13.281	12.167	11.137	10.527	9.2205
	0.15	Ω_{L1}	11.497	10.982	9.6405	8.7886	8.0410	7.3389	6.9297	6.0858
		Ω_{L2}	16.783	16.041	14.109	12.873	11.761	10.679	10.060	8.8657
		Ω_{L3}	21.659	20.709	18.216	16.602	15.134	13.708	12.913	11.426
60°	0.05	Ω_{L1}	8.6182	8.2172	7.1865	6.5606	6.0523	5.6101	5.3205	4.5939
		Ω_{L2}	15.743	15.016	13.139	11.986	11.033	10.193	9.6614	8.3781
		Ω_{L3}	15.743	15.017	13.149	12.006	11.058	10.209	9.6685	8.3781
	0.1	Ω_{L1}	14.679	14.018	12.303	11.225	10.290	9.4121	8.8890	7.7795
		Ω_{L2}	25.055	23.944	21.047	19.198	17.544	15.951	15.037	13.242
		Ω_{L3}	25.055	23.944	21.049	19.201	17.547	15.951	15.037	13.242
	0.15	Ω_{L1}	18.378	17.573	15.468	14.107	12.863	11.641	10.959	9.6939
		Ω_{L2}	29.880	28.591	25.201	22.974	20.887	18.802	17.675	15.721
		Ω_{L3}	29.880	28.591	25.209	22.991	20.911	18.818	17.682	15.721
90°	0.05	Ω_{L1}	15.453	14.743	12.911	11.784	10.845	10.002	9.4702	8.2194
		Ω_{L2}	24.582	23.465	20.582	18.795	17.269	15.851	14.981	13.051
		Ω_{L3}	29.577	28.236	24.742	22.547	20.676	18.974	17.953	15.691
	0.1	Ω_{L1}	24.232	23.165	20.377	18.586	16.965	15.385	14.493	12.794
		Ω_{L2}	36.137	34.565	30.445	27.765	25.284	22.822	21.468	19.038
		Ω_{L3}	42.422	40.584	35.747	32.574	29.626	26.711	25.127	22.333
	0.15	Ω_{L1}	28.615	27.392	24.165	22.028	19.998	17.948	16.857	15.037
		Ω_{L2}	41.198	39.447	34.821	31.734	28.767	25.752	24.171	21.619
		Ω_{L3}	47.715	45.694	40.348	36.768	33.310	29.790	27.951	25.028

method needs two type of amplitudes, the first is the specific amplitude which depends on the plate thickness, the second is the maximum amplitude to be calculated for each iteration. The new system of equations is solved using any known technique with an accuracy of around (e.g.10^{-5}).

The maximum amplitude w_{max} is evaluated as

$$w_{max} = \begin{bmatrix} N(\xi_0, \eta_0) & 0 & 0 \end{bmatrix} \begin{Bmatrix} Q_w \\ Q_{\theta_y} \\ Q_{\theta_x} \end{Bmatrix}$$
$$(i = 1, 2, \ldots (p+1)(p+2)/2) \tag{24}$$

Results

Study of convergence and comparison for linear vibration

In this part a convergence and comparison study is made for the linear vibration of clamped metallic isosceles triangular plates to validate the current formulation and methods proposed.

Table 2 shows the convergence of the first three frequencies parameter $\Omega = \omega b^2 \sqrt{\rho h/D}$ of metallic clamped isosceles triangular plate ($\beta = 90°$) for the three following different thickness ratio ($h/b = 0.05$, 0.1 and 0.15). The convergence of results can be accelerated by increasing the polynomial order p from 6 to 11. To validate the accuracy of the present solution, a comparison, listed in Table 3, is made between the present results and the results of p-version Ritz method (Liew et al. 1998) of first three linear frequency parameters for metallic clamped isosceles triangular plate, the geometric parameters of this plate are taken ($\beta = 30°$, 60° and 90°) for apex angle and ($h/b = 0.05$, 0.1 and 0.15) for thickness ratio. From this table, it can be found that the present results are in good agreement with the published results. From this

Table 7 The first three linear frequency parameters of clamped FG AL/ZrO_2 isosceles triangular plate

β	h/b	Mode	n							
			ceramic	0.1	0.5	1	2	5	10	metal
30°	0.05	Ω_{L1}	3.0021	2.9572	2.8416	2.7888	2.7883	2.8317	2.8112	2.5773
		Ω_{L2}	4.6942	4.6257	4.4505	4.3711	4.3692	4.4266	4.3896	4.0299
		Ω_{L3}	6.3787	6.2869	6.0482	5.9351	5.9251	5.9981	5.9503	5.4760
	0.1	Ω_{L1}	5.3989	5.3268	5.1359	5.0398	5.0174	5.0496	5.0015	4.6348
		Ω_{L2}	8.1325	8.0301	7.7590	7.6194	7.5751	7.5901	7.5050	6.9816
		Ω_{L3}	10.735	10.604	10.250	10.056	9.9768	9.9757	9.8654	9.2158
	0.15	Ω_{L1}	7.0850	7.0016	6.7739	6.6473	6.5896	6.5742	6.4964	6.0823
		Ω_{L2}	10.320	10.207	9.8999	9.7224	9.6219	9.5516	9.4211	8.8596
		Ω_{L3}	13.300	13.161	12.769	12.526	12.368	12.251	12.086	11.418
60°	0.05	Ω_{L1}	5.3502	5.2734	5.0781	4.9894	4.9857	5.0425	4.9975	4.5931
		Ω_{L2}	9.7566	9.6227	9.2739	9.1052	9.0780	9.1532	9.0675	8.3758
		Ω_{L3}	9.7566	9.6232	9.2816	9.1224	9.0985	9.1668	9.0741	8.3758
	0.1	Ω_{L1}	9.0573	8.9471	8.6541	8.4990	8.4407	8.4359	8.3353	7.7755
		Ω_{L2}	15.415	15.244	14.774	14.500	14.358	14.268	14.081	13.233
		Ω_{L3}	15.415	15.244	14.777	14.509	14.362	14.270	14.082	13.233
	0.15	Ω_{L1}	11.283	11.165	10.838	10.642	10.517	10.414	10.266	9.6865
		Ω_{L2}	18.297	18.125	17.627	17.299	17.040	16.784	16.532	15.707
		Ω_{L3}	18.297	18.125	17.632	17.310	17.056	16.797	16.538	15.707
90°	0.05	Ω_{L1}	9.5715	9.4422	9.1085	8.9487	8.9212	8.9816	8.8897	8.2169
		Ω_{L2}	15.196	15.003	14.502	14.254	14.185	14.215	14.050	13.045
		Ω_{L3}	18.269	18.040	17.419	17.086	16.970	17.004	16.829	15.684
	0.1	Ω_{L1}	14.892	14.732	14.291	14.033	13.882	13.769	13.580	12.785
		Ω_{L2}	22.158	21.938	21.319	20.930	20.650	20.390	20.091	19.022
		Ω_{L3}	25.992	25.741	25.014	24.537	24.177	23.847	23.505	22.313
	0.15	Ω_{L1}	17.500	17.340	16.880	16.571	16.314	16.039	15.785	15.023
		Ω_{L2}	25.157	24.943	24.305	23.848	23.428	22.966	22.596	21.596
		Ω_{L3}	29.123	28.883	28.152	27.614	27.104	26.542	26.113	25.002

table, it can be found that the present results are in good agreement with the published results.

Linear vibration of FGMs isosceles triangular plate

This part of study present the linear free vibration of thick FGMs isosceles triangular plates designed by four different mixtures (FGM 1: AL/AL_2O_3, FGM 2: $SUS304/Si_3N_4$, FGM 3: Ti-6AL-4 V/Aluminum oxide and FGM 4: AL/ZrO_2). Tables 4, 5, 6, 7 display the first three linear frequency parameters $\Omega_L = \omega b^2 \sqrt{12\rho_m(1-\nu^2)/E_m}$ for a clamped FGMs isosceles triangular plate, three apex angles ($\beta = 30°$, 60° and 90°) and three thickness ratio ($h/b = 0.05$, 0.1 and 0.15) are considered. The exponent of volume fraction vary from 0 to ∞ and it takes the values presented in tables. The results presented in this section comes to enrich the results of literatures. The tables visibly show that the linear frequency parameters is proportional to the angle and thickness and inversely proportional to the volume fraction exponent. For the triangular plate with apex angle ($\beta = 60°$), it is noted that the second and third modes are double modes for cases purely metal or purely ceramic, but varied the volume fraction exponent there is a small spacing between the two modes, the maximum spacing is the round of $n = 1$.

Non-linear vibration of isosceles triangular FG-plate

The investigation of the effects of the FGM mixtures, volume fraction exponent, thickness ratio, apex angle and boundary conditions on the hardening behavior are investigated in this part. The resultant backbone curves which shows the change in the nonlinear-to-linear frequency ratio Ω_{NL}/Ω_L according to maximum amplitude-to-thickness ratios $|w_{max}|/h$ are plotted in Figs. 2, 3, 4, 5 for clamped FG isosceles triangular plate. In Fig. 2, four different mixtures of FGM (FGM 1: AL/AL_2O_3, FGM 2: $SUS304/Si_3N_4$, FGM 3: Ti-6AL-4 V/Aluminum oxide and FGM 4: AL/ZrO_2) are considered for volume fraction exponent $n = 0.5$. The thickness ratio and the apex angle of FG isosceles triangular plate are taken respectively as $h/b = 0.1$, $\beta = 60°$. The effect of apex angle and thickness on the backbone curve for the first mode of the functionally garded AL/AL_2O_3 clamped triangular plate with ($\beta = 60°$) and $n = 1$ are presented in Figs. 3, 4. The effects of mixtures, thickness ratio and apex angle are clearly shown on the plot of these figures. The plots clearly show that if the thickness and angle increases the effects of the hardening behavior increases automatically. Also, the nonlinear vibration of the triangular plate with mixture FGM 4 presents the greatest hardening behavior compared to others mixtures of FGM.

The boundary conditions effects on the fundamental backbone curves for FG AL/AL_2O_3 isosceles triangular

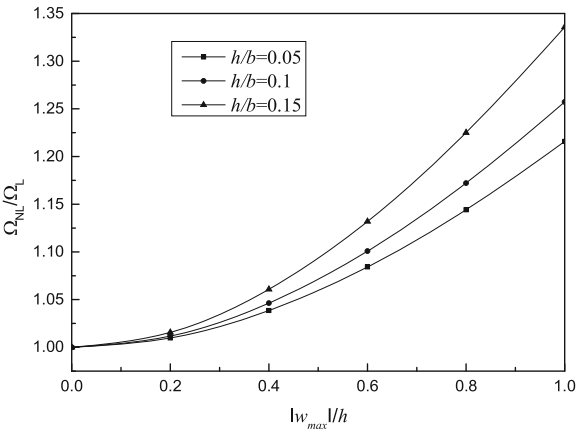

Fig. 3 The thickness effects on the fundamental backbone curves for clamped FG AL/AL_2O_3 isosceles triangular plate ($\beta = 60°$ and n =1)

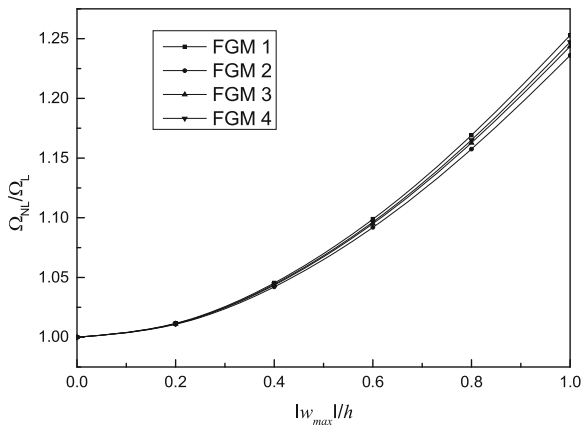

Fig. 2 Material mixtures effects on the fundamental backbone curves for clamped FG triangular plate ($\beta = 60°$, $h/b = 0.1$, $n = 0.5$)

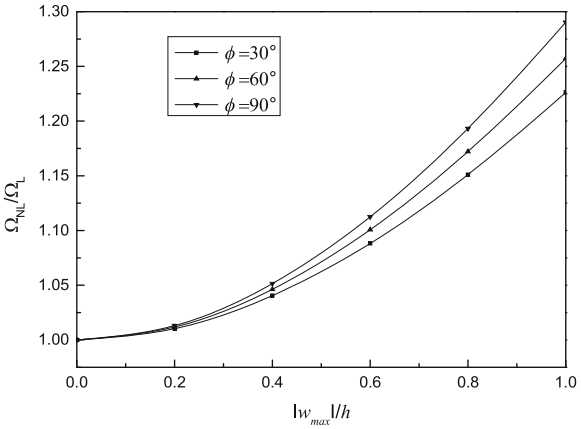

Fig. 4 The apex angle effects on the fundamental backbone curves for clamped FG AL/AL_2O_3 isosceles triangular plate ($h/b = 0.1$and $n = 1$)

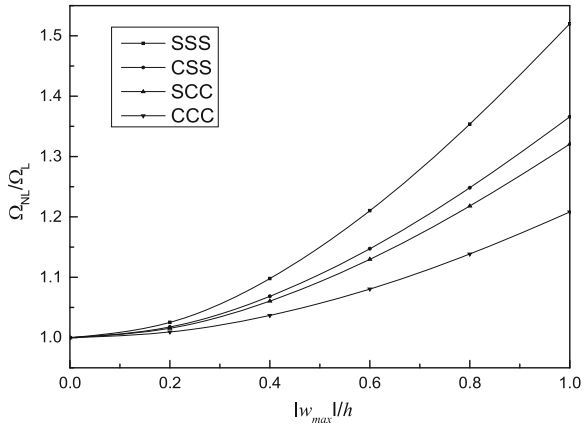

Fig. 5 The boundary conditions effects on the fundamental backbone curves for FG AL/AL_2O_3 isosceles triangular plate ($\beta = 90°$, $h/b = 0.05$ and n =1)

plate are investigated in Fig. 5. Four different boundary conditions are considered in this part of study SSS, CSS, SCC and CCC (S: simply supported edge and C : clamped edge). The volume fraction exponent, thickness ratio and the apex angle of FG isosceles triangular plate are taken respectively as n =1, $h/b = 0.05$ and $\beta = 90°$. The figure clearly show that the FG plate with simply supported boundary conditions presents a more accentuated hardening behavior than the other boundary conditions. It is noted that the hardening effect increases when the plate becomes more free (SSS) and decreases as the plate becomes more fixed (CCC), this difference in the results is due to the rotation of the edges.

The variation of frequency ratio Ω_{NL}/Ω_L according to volume fraction exponent for clamped isosceles triangular plate with four different mixtures of FGMs is shown in Fig. 6. The exponent of volume fraction take values from 0 to 20 and maximum amplitude-to-thickness

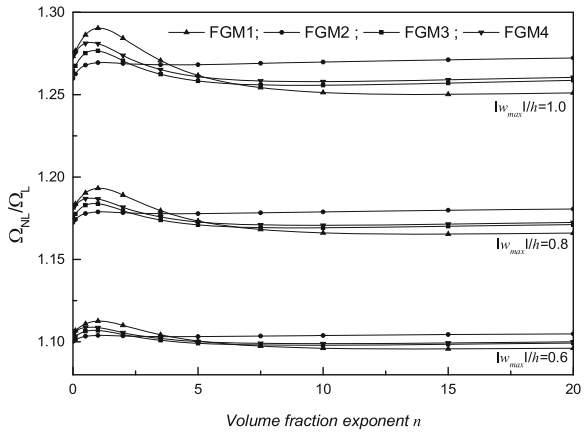

Fig. 6 Material mixtures effects on the variation of the nonlinear-to-linear fundamental frequency ratio with the volume fraction exponent for clamped FG isosceles triangular plate ($h/b = 0.1$, $\beta = 90°$)

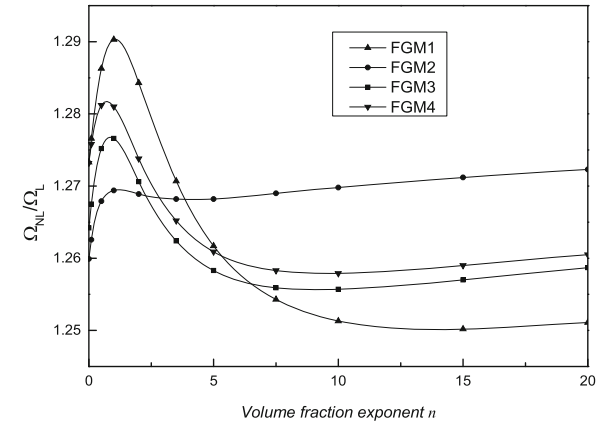

Fig. 7 Material mixtures effects on the variation of the nonlinear-to-linear fundamental frequency ratio with the volume fraction exponent for clamped FG isosceles triangular plate ($|w_{max}|/h = 1$, $h/b = 0.1$, $\beta = 90°$)

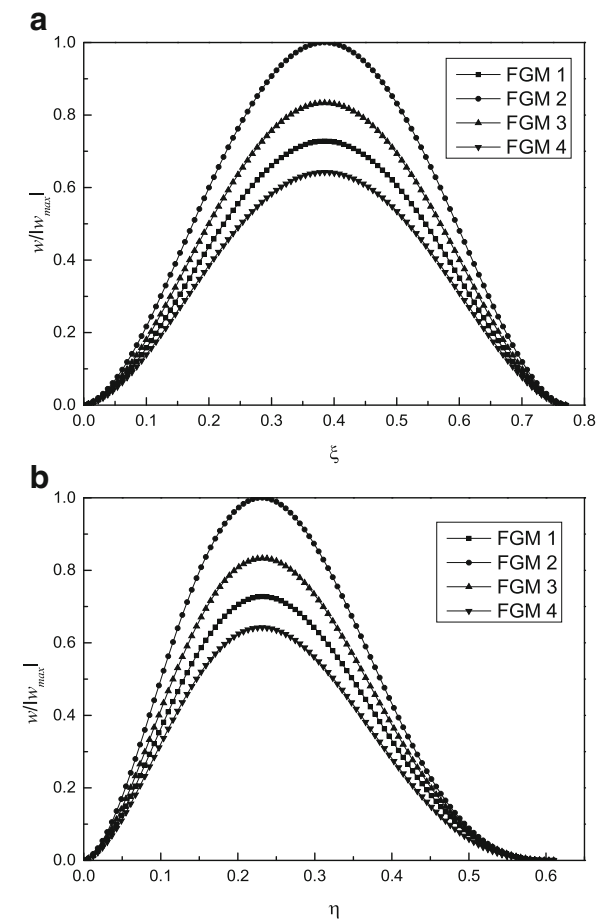

Fig. 8 Section of normalized non-linear fundamental mode shapes of FG isosceles triangular plate : **a**) along of ξ; **b**) alone of η ($\beta = 30°$, $n = 1$, $h/b = 0.05$)

ratios take three values $|w_{max}|/h = 0.6$, 0.8 and 1. The geometric parameters of the plate are ($\beta = 90°$) and h/b =0.1. Noted that the shape of the graph is similar for three values of the maximum amplitude-to-thickness ratios of this fact and to understand the phenomenon and good interpretation, Fig. 7 plot only the results of the largest value of the maximum amplitude $|w_{max}|/h = 1$. It can be seen for volume fraction exponent which varied between $n = 0$ to $n = 4$ the hardening effect is maximum for the first mixture (AL/AL_2O_3), for values $n \geq 4$ the second mixture (which $SUS304/Si_3N_4$) presents the greatest hardening effect. For third and fourth mixtures (Ti-6AL-4 V/Aluminum oxide and AL/ZrO_2) the shape of the two curves are parallel with superiority of the values obtained for the fourth mixture FGM 4. Note that the peak of the hardening behavior for four curves is obtained for volume fraction exponent $n = 1$, at which corresponds to a linear variation of constituent materials of the mixture. By comparing the spacing between curves FGM1 (Al/Al_2O_3) and FGM4 (Al/ZrO_2) we see clearly the influence of physical properties of the two ceramic (Al_2O_3 and ZrO_2) on hardening behavior. This influence is not due to metal (Al) since the same metal is used in both mixtures.

Figures 8, 9, 10 shows the normalized non-linear fundamental mode shape of isosceles triangular plate for four different mixtures of FGM along the line passes through the point of maximum amplitude (ξ_0, η_0). The mode shape are normalized by dividing by their own maximum displacement. Three apex angles and thickness ratio of FG plate are considered ($\beta =$ 30°, 60° and 90°), ($h/b = 0.05$) respectively, volume fraction exponent $n = 1$ and the maximum amplitude $|w_{max}|/h = 1$. It can see from these graphs that the displacement is maximum for the FGM 2 ($SUS304/Si_3N_4$) then comes FGM3 (Ti-6Al-4 V/Aluminum oxide) with a percentage of displacement 83% of maximum displacement, FGM 1 (AL/AL_2O_3) with 72% and lastly FGM 4 (AL/ZrO_2) with 64%. The normalized non-linear of second and third modes shape of

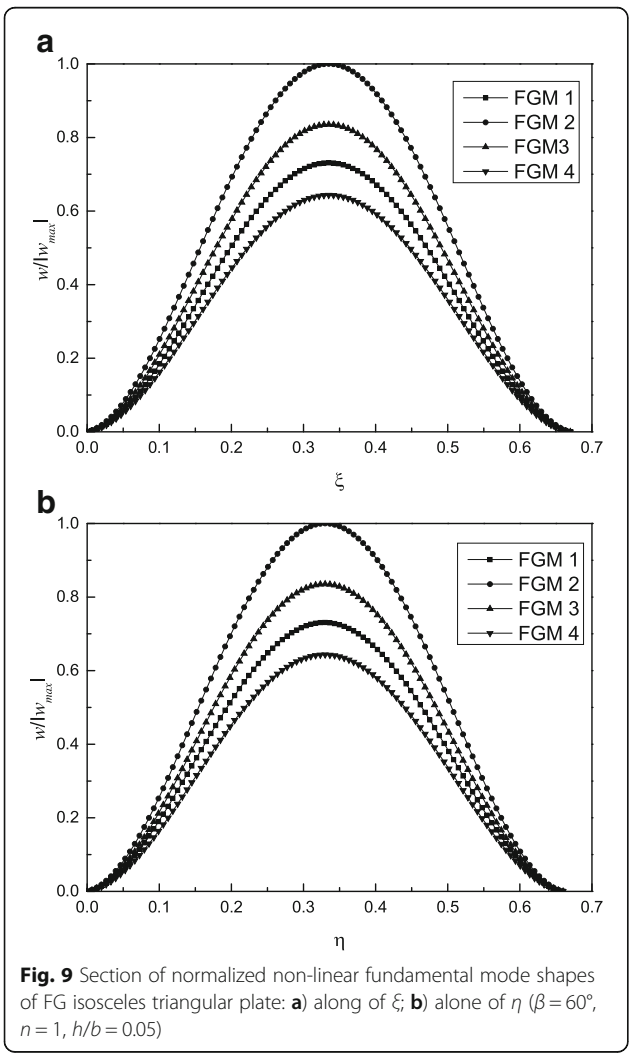

Fig. 9 Section of normalized non-linear fundamental mode shapes of FG isosceles triangular plate: **a**) along of ξ; **b**) alone of η ($\beta = 60°$, $n = 1$, $h/b = 0.05$)

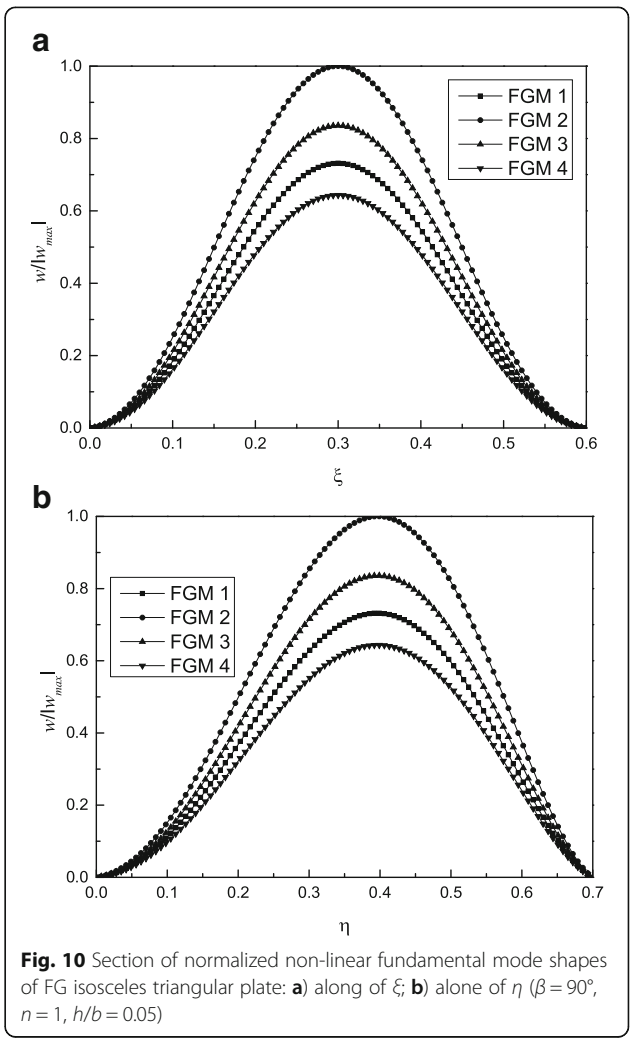

Fig. 10 Section of normalized non-linear fundamental mode shapes of FG isosceles triangular plate: **a**) along of ξ; **b**) alone of η ($\beta = 90°$, $n = 1$, $h/b = 0.05$)

isosceles triangular plates for the same mixtures used early are plotted in Figs. 11, 12, respectively. The geometric parameters used are $h/b = 0.05$, $\beta = 90°$ and $|w_{max}|/h = 0.8$. It can be seen from this plot the effect of mixtures on normalized non-linear first three fundamental mode shape of isosceles triangular plate. This is due to fact that the composition of mixtures contribute to various in-plane forces in the isosceles triangular plate.

Conclusions

The non-linear free vibration of moderately thick FGMs clamped isosceles triangular plates was analyzed by a triangular *p*-element. The material properties of the functionally graded triangular plate assumed to be graded only in the thickness direction according to a simple power law distribution in terms of the volume fraction of the constituents. The shape functions of triangular finite p-element are obtained by the shifted orthogonal polynomials of Legendre. The components of stiffness and mass matrices were calculated using numerical integration of Gauss-Legendre. The equations of motion are obtained from Lagrange's equation in combination with the harmonic balance method (HBM). Results for linear and non-linear frequency for the lowest three modes of FGMs clamped isosceles triangular plates were obtained. The parametric studies show that the boundary conditions have a great influence on the shape of the backbone curves, the hardening spring effect decreases for clamped FG plate. For simply supported FG plate and by increasing thickness ratio and sector angle of FG plates the hardening spring effect increases. A increase in the volume fraction exponent produces a variation in the hardening spring effect with an increasing part and another decreasing part, the peak in the curves of the nonlinear-to-linear fundamental frequency ratio FG triangular plate is obtained around of n = 1 at which the hardening behavior is maximum, and is obtained for AL/AL_2O_3 FG plate. This value of volume fraction exponent corresponds

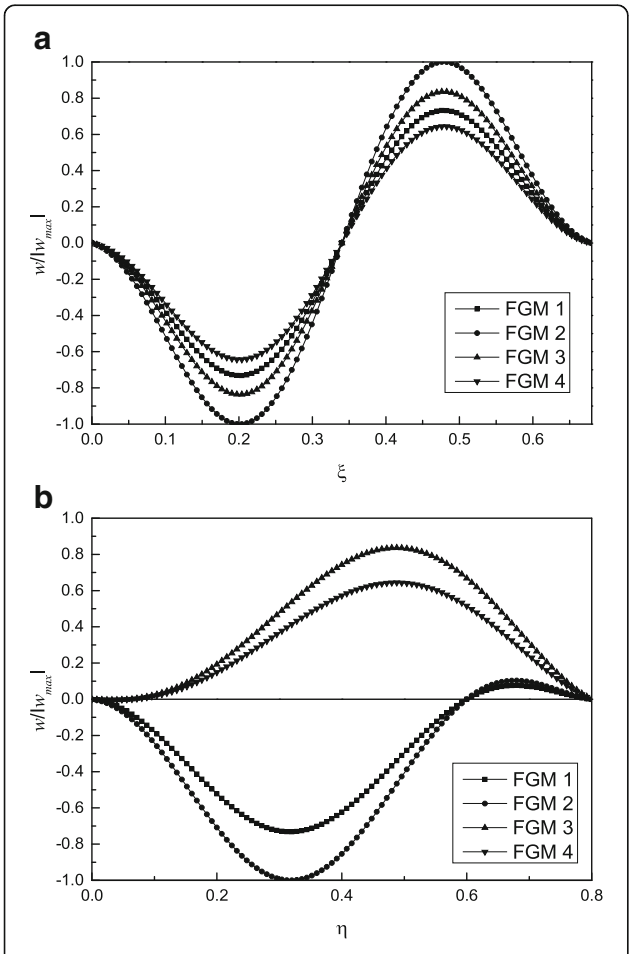

Fig. 11 Section of normalized non-linear second mode shapes of FG isosceles triangular plate: **a**) along of ξ; **b**) alone of η ($\beta = 90°$, $n = 1$, $h/b = 0.05$)

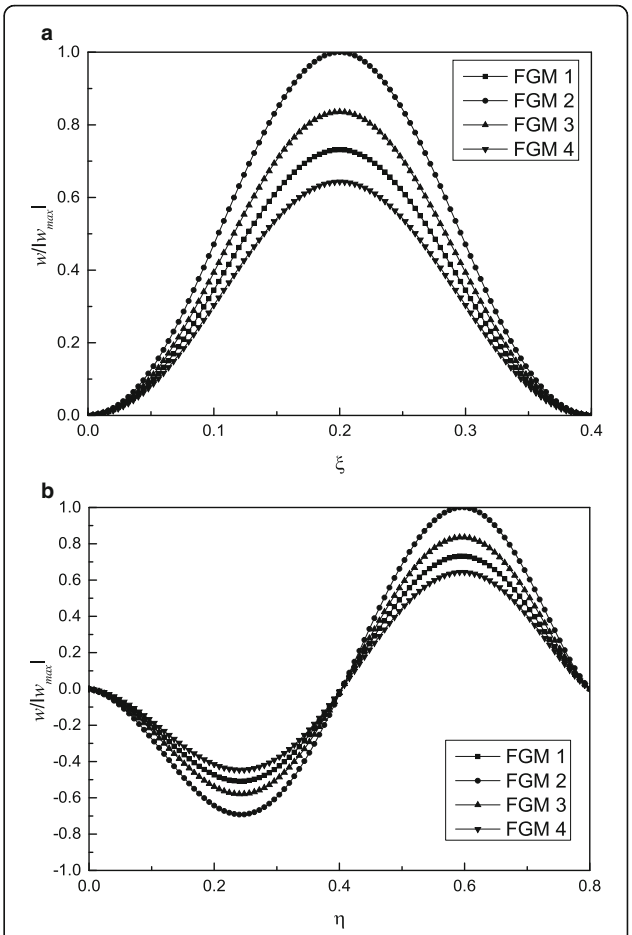

Fig. 12 Section of normalized non-linear third mode shapes of FG isosceles triangular plate: **a**) along of ξ; **b**) alone of η ($\beta = 90°$, $n = 1$, $h/b = 0.05$)

to equal mixtures of metal and ceramic in the composition of the FG plate. Not only the hardening behavior is influenced by this mixture but the nonlinear mode shape of FG isosceles triangular plate is also influenced.

Appendix A

$$\overline{\mathbf{K}}_{\alpha,\beta} = \begin{bmatrix} \overline{K}_{2\alpha-1,2\beta-1} & \overline{K}_{2\alpha-1,2\beta} \\ \overline{K}_{2\alpha,2\beta-1} & \overline{K}_{2\alpha,2\beta} \end{bmatrix} \tag{A.1}$$

$$\mathbf{K}_{\alpha,\beta} = \begin{bmatrix} K_{3\alpha-2,3\beta-2} & K_{3\alpha-2,3\beta-1} & K_{3\alpha-2,3\beta} \\ K_{3\alpha-1,3\beta-2} & K_{3\alpha-1,3\beta-1} & K_{3\alpha-1,3\beta} \\ K_{3\alpha,3\beta-2} & K_{3\alpha,3\beta-1} & K_{3\alpha,3\beta} \end{bmatrix} \tag{A.2}$$

$$\mathbf{M}_{\alpha,\beta} = \begin{bmatrix} M_{3\alpha-2,3\beta-2} & M_{3\alpha-2,3\beta-1} & M_{3\alpha-2,3\beta} \\ M_{3\alpha-1,3\beta-2} & M_{3\alpha-1,3\beta-1} & M_{3\alpha-1,3\beta} \\ M_{3\alpha,3\beta-2} & M_{3\alpha,3\beta-1} & M_{3\alpha,3\beta} \end{bmatrix} \tag{A.3}$$

$$\hat{\mathbf{K}}_{\alpha,\beta} = \begin{bmatrix} \hat{K}_{2\alpha-1,3\beta-2} & \hat{K}_{2\alpha-1,3\beta-1} & \hat{K}_{2\alpha-1,3\beta} \\ \hat{K}_{2\alpha,3\beta-2} & \hat{K}_{2\alpha,3\beta-1} & \hat{K}_{2\alpha,3\beta} \end{bmatrix} \tag{A.4}$$

$$\breve{\mathbf{K}}_{\alpha,\beta} = \begin{bmatrix} \breve{K}_{2\alpha-1,3\beta-2} & \breve{K}_{2\alpha-1,3\beta-1} & \breve{K}_{2\alpha-1,3\beta} \\ \breve{K}_{2\alpha,3\beta-2} & \breve{K}_{2\alpha,3\beta-1} & \breve{K}_{2\alpha,3\beta} \end{bmatrix} \tag{A.5}$$

$$\tilde{\mathbf{K}}_{\alpha,\beta} = \begin{bmatrix} \tilde{K}_{3\alpha-2,3\beta-2} & \tilde{K}_{3\alpha-2,3\beta-1} & \tilde{K}_{3\alpha-2,3\beta} \\ \tilde{K}_{3\alpha-1,3\beta-2} & \tilde{K}_{3\alpha-1,3\beta-1} & \tilde{K}_{3\alpha-1,3\beta} \\ \tilde{K}_{3\alpha,3\beta-2} & \tilde{K}_{3\alpha,3\beta-1} & \tilde{K}_{3\alpha,3\beta} \end{bmatrix} \tag{A.6}$$

The non-zero elements of the matrices M, **K**, $\overline{\mathrm{K}}$, $\hat{\mathrm{K}}$, $\breve{\mathrm{K}}$ and $\tilde{\mathrm{K}}$ are expressed as

$$M_{3\,\alpha-2,3\beta-2} = \int_0^1 \int_0^{1-\xi} I_1 N_\alpha N_\beta |\mathbf{J}| \,\mathrm{d}\xi \,\mathrm{d}\eta \tag{A.7}$$

$$M_{3\,\alpha-1,3\beta-1} = M_{3\,\alpha,3\beta} = \int_0^1 \int_0^{1-\xi} I_3 N_\alpha N_\beta |\mathbf{J}| \,\mathrm{d}\xi \,\mathrm{d}\eta \tag{A.8}$$

$$K_{3\alpha-2,3\beta-2} = \int_0^1 \int_0^{1-\xi} k \left(A_{44} \frac{\partial N_\alpha}{\partial \xi} \frac{\partial N_\beta}{\partial \xi} + A_{55} \frac{\partial N_\alpha}{\partial \eta} \frac{\partial N_\beta}{\partial \eta} \right) |\mathbf{J}| \,\mathrm{d}\xi \,\mathrm{d}\eta \tag{A.9}$$

$$K_{3\alpha-2,3\beta-1} = -\int_0^1 \int_0^{1-\xi} k A_{44} \frac{\partial N_\alpha}{\partial \eta} N_\beta |\mathbf{J}| \,\mathrm{d}\xi \,\mathrm{d}\eta \tag{A.10}$$

$$K_{3\alpha-2,3\beta} = \int_0^1 \int_0^{1-\xi} k A_{55} \frac{\partial N_\alpha}{\partial \xi} N_\beta |\mathbf{J}| \,\mathrm{d}\xi \,\mathrm{d}\eta \tag{A.11}$$

$$K_{3\alpha-1,3\beta-2} = -\int_0^1 \int_0^{1-\xi} k A_{44} N_\alpha \frac{\partial N_\beta}{\partial \eta} |\mathbf{J}| \,\mathrm{d}\xi \,\mathrm{d}\eta \tag{A.12}$$

$$K_{3\alpha-1,3\beta-1} = \int_0^1 \int_0^{1-\xi} \left(D_{22} \frac{\partial N_\alpha}{\partial \eta} \frac{\partial N_\beta}{\partial \eta} + D_{66} \frac{\partial N_\alpha}{\partial \xi} \frac{\partial N_\beta}{\partial \xi} + k A_{44} N_\alpha N_\beta \right) |\mathbf{J}| \,\mathrm{d}\xi \,\mathrm{d}\eta \tag{A.13}$$

$$K_{3\alpha-1,3\beta} = -\int_0^1 \int_0^{1-\xi} \left(D_{12} \frac{\partial N_\alpha}{\partial \eta} \frac{\partial N_\beta}{\partial \xi} + D_{66} \frac{\partial N_\alpha}{\partial \xi} \frac{\partial N_\beta}{\partial \eta} \right) |\mathrm{J}| \,\mathrm{d}\xi \,\mathrm{d}\eta \tag{A.14}$$

$$K_{3\alpha,3\beta-2} = \int_0^1 \int_0^{1-\xi} k A_{55} N_\alpha \frac{\partial N_\beta}{\partial \eta} |\mathbf{J}| \,\mathrm{d}\xi \,\mathrm{d}\eta \tag{A.15}$$

$$K_{3\alpha,3\beta-1} = -\int_0^1 \int_0^{1-\xi} \left(D_{12} \frac{\partial N_\alpha}{\partial \xi} \frac{\partial N_\beta}{\partial \eta} + D_{66} \frac{\partial N_\alpha}{\partial \eta} \frac{\partial N_\beta}{\partial \xi} \right) |\mathbf{J}| \,\mathrm{d}\xi \,\mathrm{d}\eta \tag{A.16}$$

$$K_{3\alpha,3\beta} = \int_0^1 \int_0^{1-\xi} \left(D_{11} \frac{\partial N_\alpha}{\partial \xi} \frac{\partial N_\beta}{\partial \xi} + D_{66} \frac{\partial N_\alpha}{\partial \eta} \frac{\partial N_\beta}{\partial \eta} + k A_{55} N_\alpha N_\beta \right) |\mathbf{J}| \,\mathrm{d}\xi \,\mathrm{d}\eta \tag{A.17}$$

$$\overline{K}_{2\alpha-1,2\beta-1} = \int_0^1 \int_0^{1-\xi} \left(A_{11} \frac{\partial N_\alpha}{\partial \xi} \frac{\partial N_\beta}{\partial \xi} + A_{66} \frac{\partial N_\alpha}{\partial \eta} \frac{\partial N_\beta}{\partial \eta} \right) |\mathbf{J}| \,\mathrm{d}\xi \,\mathrm{d}\eta \tag{A.18}$$

$$\overline{K}_{2\alpha-1,2\beta} = \int_0^1 \int_{0^{1-\xi}} \left(A_{12} \frac{\partial N_\alpha}{\partial \xi} \frac{\partial N_\beta}{\partial \eta} + A_{66} \frac{\partial N_\alpha}{\partial \eta} \frac{\partial N_\beta}{\partial \xi} \right) |\mathbf{J}| \,\mathrm{d}\xi \,\mathrm{d}\eta \tag{A.19}$$

$$\overline{K}_{2\alpha,2\beta-1} = \int_0^1 \int_0^{1-\xi} \left(A_{12} \frac{\partial N_\alpha}{\partial \eta} \frac{\partial N_\beta}{\partial \xi} + A_{66} \frac{\partial N_\alpha}{\partial y} \frac{\partial N_\beta}{\partial \eta} \right) |\mathbf{J}| \,\mathrm{d}\xi \,\mathrm{d}\eta \tag{A.20}$$

$$\overline{K}_{2\alpha,2\beta} = \int_0^1 \int_0^{1-\xi} \left(A_{22} \frac{\partial N_\alpha}{\partial \eta} \frac{\partial N_\beta}{\partial \eta} + A_{66} \frac{\partial N_\alpha}{\partial \xi} \frac{\partial N_\beta}{\partial \xi} \right) |\mathbf{J}| \,\mathrm{d}\xi \,\mathrm{d}\eta \tag{A.21}$$

$$\hat{K}_{2\alpha-1,3\beta-2} = \frac{1}{2} \sum_{\delta=1}^{r} \left(\int_0^1 \int_0^{1-\xi} \left(A_{11} \frac{\partial N_\alpha}{\partial \xi} \frac{\partial N_\beta}{\partial \xi} \frac{\partial N_\delta}{\partial \xi} + A_{12} \frac{\partial N_\alpha}{\partial \xi} \frac{\partial N_\beta}{\partial \eta} \frac{\partial N_\delta}{\partial \eta} + 2A_{66} \frac{\partial N_\alpha}{\partial \eta} \frac{\partial N_\beta}{\partial \xi} \frac{\partial N_\delta}{\partial \eta} \right) |\mathbf{J}| \,\mathrm{d}\xi \,\mathrm{d}\eta \right) Q_{3\delta-2} \tag{A.22}$$

$$\hat{K}_{2\alpha,3\beta-2} = \frac{1}{2}\sum_{\delta=1}^{r}\left(\int_0^1\int_0^{1-\xi}\left(A_{22}\frac{\partial N_\alpha}{\partial\eta}\frac{\partial N_\beta}{\partial\eta}\frac{\partial N_\delta}{\partial\eta} + A_{12}\frac{\partial N_\alpha}{\partial\eta}\frac{\partial N_\beta}{\partial\xi}\frac{\partial N_\delta}{\partial\xi} + 2A_{66}\frac{\partial N_\alpha}{\partial\xi}\frac{\partial N_\beta}{\partial\xi}\frac{\partial N_\delta}{\partial\eta}\right)|\mathbf{J}|\,\mathrm{d}\xi\,\mathrm{d}\eta\right) Q_{3\delta-2} \tag{A.23}$$

$$\breve{K}_{2\alpha-1,3\beta-1} = \int_0^1\int_0^{1-\xi}\left(B_{12}\frac{\partial N_\alpha}{\partial\xi}\frac{\partial N_\beta}{\partial\eta} - B_{66}\frac{\partial N_\alpha}{\partial\eta}\frac{\partial N_\beta}{\partial\xi}\right)|\mathbf{J}|\,\mathrm{d}\xi\,\mathrm{d}\eta \tag{A.24}$$

$$\breve{K}_{2\alpha-1,3\beta} = \int_0^1\int_{0^{1-\xi}}\left(B_{11}\frac{\partial N_\alpha}{\partial\xi}\frac{\partial N_\beta}{\partial\eta} + B_{66}\frac{\partial N_\alpha}{\partial\eta}\frac{\partial N_\beta}{\partial\xi}\right)|\mathbf{J}|\,\mathrm{d}\xi\,\mathrm{d}\eta \tag{A.25}$$

$$\breve{K}_{2\alpha,3\beta-1} = \int_0^1\int_0^{1-\xi}\left(B_{22}\frac{\partial N_\alpha}{\partial\eta}\frac{\partial N_\beta}{\partial\eta} - B_{66}\frac{\partial N_\alpha}{\partial\xi}\frac{\partial N_\beta}{\partial\xi}\right)|\mathbf{J}|\,\mathrm{d}\xi\,\mathrm{d}\eta \tag{A.26}$$

$$\breve{K}_{2\alpha,3\beta} = \int_0^1\int_0^{1-\xi}\left(B_{12}\frac{\partial N_\alpha}{\partial\eta}\frac{\partial N_\beta}{\partial\xi} + B_{66}\frac{\partial N_\alpha}{\partial\xi}\frac{\partial N_\beta}{\partial\eta}\right)|\mathbf{J}|\,\mathrm{d}\xi\,\mathrm{d}\eta \tag{A.27}$$

$$\tilde{K}_{3\alpha-2,3\beta-2} = \frac{1}{2}\sum_{\delta=1}^{r}\sum_{\gamma=1}^{r}\left(\int_0^1\int_0^{1-\xi}\left(A_{11}\frac{\partial N_\alpha}{\partial\xi}\frac{\partial N_\beta}{\partial\xi}\frac{\partial N_\delta}{\partial\xi}\frac{\partial N_\gamma}{\partial\xi} + A_{22}\frac{\partial N_\alpha}{\partial\eta}\frac{\partial N_\beta}{\partial\eta}\frac{\partial N_\delta}{\partial\eta}\frac{\partial N_\gamma}{\partial\eta} + (A_{12}+2A_{66})\frac{\partial N_\alpha}{\partial\xi}\frac{\partial N_\beta}{\partial\xi}\frac{\partial N_\delta}{\partial\eta}\frac{\partial N_\gamma}{\partial\eta} + (A_{12}+2A_{66})\frac{\partial N_\alpha}{\partial\eta}\frac{\partial N_\beta}{\partial\eta}\frac{\partial N_\delta}{\partial\xi}\frac{\partial N_\gamma}{\partial\xi}\right)|\mathbf{J}|\,\mathrm{d}\xi\,\mathrm{d}\eta\right) Q_{3\delta-2}, Q_{3\gamma-2} \tag{A.28}$$

Competing interests
The author declare no significant competing financial, professional or personal interests that might have influenced the performance or presentation of the work described in this manuscript.

Author details
Laboratory of Computational Mechanics, Faculty of Technology, Department of Mechanical Engineering, University of Tlemcen, B.P. 230, Tlemcen 13000, Algeria.

Received: 2 September 2016 Accepted: 12 January 2017
Published online: 01 February 2017

References

Alinaghizadeh F, Shariati M (2016) Geometrically non-linear bending analysis of thick two-directional functionally graded annular sector and rectangular plates with variable thickness resting on non-linear elastic foundation. Compos Part B 86:61–83
Allahverdizadeh A, Naei MH, Bahrami MN (2008a) Nonlinear free and forced vibration analysis of thin circular functionally graded plates. J Sound Vib 310: 966–984
Allahverdizadeh A, Naei MH, Bahrami MN (2008b) Vibration amplitude and thermal effects on nonlinear behavior of thin circular functionally graded plates. Int J Mech Sci 50:445–454
Belalia SA, Houmat A (2010) Nonlinear free vibration of elliptic sector plates by a curved triangular *p*-element. Thin-Walled Struct 48:316–326
Belalia SA, Houmat A (2012) Nonlinear free vibration of functionally graded shear deformable sector plates by a curved triangular *p*-element. Eur J Mech A Solids 35:1–9
Chen CS (2005) Nonlinear vibration of a shear deformable functionally graded plate. Compos Struct 68:295–302
Duc ND, Cong PH (2013) Nonlinear dynamic response of imperfect symmetric thin S-FGM plate with metal–ceramic–metal layers on elastic foundation. J Vib Control 21:637–646
Han W, Petyt M (1997) Geometrically nonlinear vibration analysis of thin, rectangular plates using the hierarchical finite element method-I: The fundamental mode of isotropic plates. Comput Struct 63:295–308
Hao YX, Zhang W, Yang J (2011) Nonlinear oscillation of a cantilever FGM rectangular plate based on third-order plate theory and asymptotic perturbation method. Compos Part B 42:3,402–413
Huang XL, Shen HS (2004) Nonlinear vibration and dynamic response of functionally graded plates in a thermal environment. Int J Solids Struct 41: 2403–2427
Koizumi M (1993) The concept of FGM: functionally gradient material. Ceram Trans 34:3–10
Koizumi M (1997) FGM activities in Japan. Compos Part B 28:1–4
Liew KM, Wang CM, Xiang Y, Kitipornchai S. Vibration of Mindlin plates: programming the *p*-version Ritz method. Elsevier: 1998.
Mindlin RD (1951) Influence of rotary inertia and shear on flexural vibrations of isotropic, elastic plates. J Appl Mechanics 12:69–77
Reddy JN (2000) Analysis of functionally graded plates. Int J Numer Methods Eng 47:663–684
Reddy JN, Chin CD (1998) Thermo-mechanical analysis of functionally graded cylinders and plates. J Therm Stresses 21:593–626
Reddy JN, Wang CM, Kitipornchai S (1999) Axisymmetric bending of functionally graded circular and annular plates. Eur J Mech A Solids 18:185–199
Ribeiro P (2003) A hierarchical finite element for geometrically nonlinear vibration of thick plates. Meccanica 38:115–130
Shen HS (2002) Nonlinear bending response of functionally graded plates subjected to transverse loads and in thermal environments. Int J Mech Sci 44:561–584
Woo J, Meguid SA (2001) Nonlinear behavior of functionally graded plates and shallows shells. Int J Solids Struct 38:7409–7421
Woo J, Meguid SA, Ong LS (2006) Nonlinear free vibration behavior of functionally graded plates. J Sound Vib 289:595–611
Yang J, Kitipornchai S, Liew KM (2003) Large amplitude vibration of thermo-electro-mechanically stressed FGM laminated plates Comput. Methods Appl Mech Engrg 192:3861–3885
Yin S, Yu T, Bui TQ, Nguyen MN (2015) Geometrically nonlinear analysis of functionally graded plates using isogeometric analysis. Eng Computation 32(2):519–558
Yu T, Yin S, Bui TQ, Hirose S (2015) A simple FSDT-based isogeometric analysis for geometrically nonlinear analysis of functionally graded plates. Finite Elem Anal Des 96:1–10
Zhao X, Lee YY, Liew KM (2009) Free vibration analysis of functionally graded plates using the element-free kp-Ritz method. J Sound Vib 319:918–939